Association of muscarinic M(3) receptors and Kir6.1 with caveolae in human detrusor muscle.

Ekman, Mari; Rippe, Catarina; Sadegh, Mardjaneh Karbalaei; Dabestani, Saeed; Mörgelin, Matthias; Uvelius, Bengt; Swärd, Karl

Published in:
European Journal of Pharmacology

DOI:
10.1016/j.ejphar.2012.02.039

2012

Association of muscarinic M_3 receptors and Kir6.1 with caveolae in human detrusor muscle

Mari Ekman[1*], Catarina Rippe[1*], Mardjaneh Karbalaei Sadegh[1], Saeed Dabestani[2], Matthias Mörgelin[3], Bengt Uvelius[2], Karl Swärd[1]

[1]From the Department of Experimental Medical Science, Lund University, Biomedical Centre, BMC D12, SE-221 84 Lund, Sweden; [2]Department of Urology, Clinical Sciences, Lund University, SE-221 84 Lund, Sweden; [3]Department of Infection Medicine, Clinical Sciences, Lund University, SE-221 84 Lund, Sweden

* These authors contributed equally and their names appear in alphabetical order

Number of words: 5895

Correspondence:
Dr. Karl Swärd
Department of Experimental Medical Science
Lund University
BMC D12
SE-221 84 Lund, Sweden
Tel: +46-46-2220631
Fax: +46-46-2113417
E-mail: karl.sward@med.lu.se

ABSTRACT

Caveolae are 50-100 nm large membrane invaginations that play a role in cellular signaling. The aim of the present study was to assess whether muscarinic M_3 receptors and the K_{ATP} channel subunit Kir6.1 are associated with human detrusor caveolae, and to pharmacologically assess the relevance of this organization for contractility. Detrusor strips were dissected and used in ultrastructural, biochemical and mechanical studies. Caveolae were manipulated by cholesterol desorption using methyl-β-cyclodextrin (mβcd). Mβcd disrupted caveolae and caused a cholesterol-dependent ~3-fold rightward shift of the concentration-response curve for the muscarinic receptor agonist carbachol. The effect of mβcd was inhibited by the K_{ATP} blockers glibenclamide, repaglinide and PNU-37883, and it was mimicked by the K_{ATP} activator levcromakalim. Immunoelectron microscopy showed muscarinic M_3 receptors and Kir6.1 to be enriched in caveolae. In conclusion, pharmacological K_{ATP} channel inhibition antagonizes the effect of caveolae disruption on muscarinic contractility in the human detrusor, and the K_{ATP} channel subunit Kir6.1 co-localizes with M_3 receptors in caveolae.

Key words: carbachol, detrusor, glibenclamide, cyclodextrin, smooth muscle

1. Introduction

Caveolae are 50-100 nm large plasma membrane invaginations (Cohen et al., 2004). The density of caveolae is high in smooth muscle cells and the organelles are often arranged in parallel longitudinally oriented strands (Gabella, 1976; Gabella and Blundell, 1978; North et al., 1993). Formation of caveolae depends on caveolin and cavin proteins (Cohen et al., 2004; Hill et al., 2008; Bastiani et al., 2009). Caveolins and cavin-1 are expressed in detrusor smooth muscle (Woodman et al., 2004; Shakirova et al., 2010a; Sadegh et al., 2011). Biochemical purification has revealed that signaling proteins such as mono- and heterotrimeric G-proteins and tyrosine kinases are enriched in caveolae (Chang et al., 1994). Some G protein-coupled receptors similarly reside there (Chun et al., 1994). Recently, a nanoscale labeling technique was used to demonstrate an enrichment of PtdIns 4,5-P_2 at the rims of caveolae in mouse detrusor (Fujita et al., 2009). Such examples of heterogeneous membrane distribution of signaling molecules are cornerstones of the "caveolae signaling hypothesis" which postulates that caveolae modulate the coupling of receptors to downstream signaling effectors (Lisanti et al., 1994; Shaul and Anderson, 1998).

Cholinergic activation of the urinary bladder is mediated by muscarinic M_3 receptors (Matsui et al., 2000; Fry et al., 2010; Andersson, 2011), and accumulating evidence implicates a role of caveolae in M_3 signaling. Using fluorescence microscopy and fractionation Gosens et al. (2007) showed that M_3 receptors are localized in caveolae domains in human airway smooth muscle cells, and that disruption of caveolae impairs contraction and Ca^{2+} responses at submaximal concentrations of acetylcholine. In addition, disorganization of caveolae arrays by β-dystroglycan silencing displaced caveolin-1 with associated effects on metacholin-induced Ca^{2+} signaling (Sharma et al., 2010). In accord with these findings, disruption of the

caveolin-1 gene leads to impairment of cholinergic contractility in the mouse bladder (Woodman et al., 2004; Lai et al., 2004; Sadegh et al., 2011). Desorption of cholesterol, which disrupts caveolae (Rothberg et al., 1992; Dreja et al., 2002), moreover inhibits nerve- and carbachol-induced contraction in the human bladder (Shakirova et al., 2010a). The exact mechanism by which caveolae modulate muscarinic signaling is however unclear.

Studies in rat arterial smooth muscle have shown that K_{ATP} channels, consisting of Kir6.1 and SUR2B, are localized in caveolae (Sampson et al., 2004; Sampson et al., 2007). Caveolin-1 impairs K_{ATP} activation by MgADP in HEK293 cells (Davies et al., 2010). K_{ATP} channels are expressed in the human detrusor, and their pharmacological activation relaxes muscarinic contraction (Aishima et al., 2006). Electrophysiological experiments using the guinea pig detrusor have shown that muscarinic receptor stimulation leads to inhibition of K_{ATP} current via protein kinase C (PKC) (Bonev and Nelson, 1993). Because human detrusor K_{ATP} channels appear to have a molecular composition similar to the corresponding channels in vascular smooth muscle (Kajioka et al., 2011), we hypothesized that they are associated with caveolae, and that they are involved in the effect of caveola disruption on muscarinic contractility. Our objective was to test this hypothesis using pharmacological experiments and immunoelectron microscopy.

2. Material and methods

2.1. Detrusor preparation

Transmural specimens were cut from the healthy part of the bladder after radical cystectomy for localized urothelial cancer and transported to the laboratory in Ca^{2+}-free HEPES buffered Krebs solution (composition in mM: NaCl 135.5, KCl 5.9, $MgCl_2$ 1.2, glucose 11.6, HEPES 11.6, pH 7.4) on ice. All patients (45 males and 12 females, median age 72 years) gave informed consent and experiments were approved by the regional human ethics committee. 1x1x10 mm large muscle bundles were prepared by dissection in Ca^{2+}-free HEPES buffered Krebs solution. For Western blotting muscle bundles were directly frozen in liquid nitrogen.

2.2. Conventional electron microscopy

6 bladder strips from one individual were used. Two strips were fixed after equilibration in HEPES-buffered Krebs solution at 37^{o}C for 2h (controls); two strips were fixed after 1h in HEPES buffered Krebs followed by 1h in mβcd (1h depletion, 10 mM, 37^{o}C); and two were fixed after 2h in mβcd (2h depletion, 10 mM). The fixative contained 2.5% glutaraldehyde in 150 mM sodium cacodylate buffer (pH 7.4, room temperature). Specimens were fixed for 2 hrs, followed by post-fixation in 1% osmium tetroxide, block-staining with uranyl acetate, and embedding in Araldite. Semi-thin cross sections were examined and areas were chosen and cut for transmission electron microscopy using a JEOL 1230 microscope (Jeol, Tokyo, Japan). Caveolar morphometry was determined on 60K digital photos using ImageJ (NIH, Bethesda, MD, USA).

2.3. Force recording

6-0 silk loops were tied at the ends of 1x1x3 mm preparations followed by mounting in four-channel myographs (610M, Danish Myo Technology, Aarhus, Denmark). Force data was

digitized and acquired using the WinDaq system. Preparations were allowed to equilibrate for 30 min in aerated HEPES buffered Krebs (in mM: NaCl 135.5, KCl 5.9, $MgCl_2$ 1.2, glucose 11.6, HEPES 11.6, $CaCl_2$ 2.5, pH 7.4) for 30 min at 37 ^{o}C. A basal tension of 8 mN was applied and preparations were contracted twice with 60 mM K^+ (obtained by exchange of NaCl and KCl). Following relaxation from the second contraction the preparations were either incubated for 1 h in fresh HEPES buffer or with 10 mM methyl-β-cyclodextrin (mβcd) dissolved directly in the physiological buffer in a pair-wise fashion. Responses were normalized to the second reference (high K^+, HK in the figures) contraction. Carbachol was prepared as a stock solution (10^{-2} M) followed by serial dilutions in physiological buffer. After mβcd treatment and three washes, concentration-response curves were generated by cumulative addition of carbachol ($10^{-8} \rightarrow 10^{-5}$ M). Each concentration was maintained for 7 min and analyses were made by force integration over this period.

2.4. Experimental design

In the mechanical experiments 12 preparations from one patient were mounted and cholesterol was depleted from every second preparation. Half of the control preparations and half of the depleted preparations were then drug-treated. The remaining preparations were treated with vehicle. Data from the identically treated strips in each experiment was averaged and entered into the spreadsheets as n=1. Except when indicated, n therefore refers to the number of patients. This design was chosen to allow for pairwise comparisons of the rightward shift in the presence and absence of drug in the same individual.

2.5. Sucrose gradient fractionation

Detrusor strips were frozen in liquid nitrogen and crushed to a powder that was further homogenized in lysis buffer (40 mM HEPES, 1% Triton-X, 10 mM NaF, 1 mM PMSF, 0.25

mM vanadate and protease inhibitors, pH 7.4). The homogenate was left on ice for 1h with homogenization every 15 min. After centrifugation at 5000g (7 min) the supernatant was mixed with 0.5 M Na_2CO_3 (pH 11) and sonicated on ice. An equal volume of 90% sucrose (25 mM MES and 0.15 M NaCl) was added and a discontinuous sucrose gradient was layered on top (4 ml 35% sucrose, 4 ml 5% sucrose) followed by centrifugation. Equal volumes of each fraction were loaded on SDS-PAGE gels followed by Western blotting (Sadegh et al., 2011) using antibodies against caveolin-1 (BD610407, BD Biosciences, 1:20000), human M_3 (H-210, Santa Cruz Biotechnology Inc. 1:500), Kir6.1 (R-14, sc-11224, Santa Cruz Biotechnology Inc., Sampson et al., 2007 1:200), and SM22α (transgelin, ab14106, Abcam, 1:5000).

2.6. Quantitative reverse transcription PCR (RT-qPCR)

Biopsies transported to the lab in RNAlater (Qiagen, Valencia, CA, USA) were frozen in liquid nitrogen after further dissection of bundles in RNA later. Tissue was homogenized in TRIzol® (Invitrogen) with an Omni homogenizor (Omni International, Kennesaw, USA). Homogenates were centrifuged and RNA isolated using RNeasy Mini Kit (Qiagen, Valencia, CA, USA). The purity and concentration of RNA was determined using a ND-1000 spectrophotometer (Nanodrop Technologies Inc. Wilmington, USA). 1µg RNA was transcribed to cDNA with Precision qScriptTM Reverse transcription kit (Primer Design, Southampton,UK). Expression levels for Kir 6.1 and Kir 6.2 were determined using SYBR green quantitative Real-Time PCR (M3000P Stratagene, La Jolla, CA, USA). Amplification was initiated by incubation at 95 ºC for 10 min, followed by 45 cycles between 95 ºC for 20 s, and 60 ºC for 1 min. The protocol was ended by incubation for 1 min at 95 ºC, 1 min at 55 ºC, and 30 s at 95 ºC and the reaction volume was 20 µl. Kir6.1 expression was related to Kir6.2 expression in the same sample using the $2^{-\Delta\Delta Ct}$ formula. Primer dimers and other unspecific

artifacts were evaluated by melting curve analysis. Primers for Kir6.1, Kir6.2, SUR1 and pan-SUR2 were from Qiagen. Additional primers for Kir6.x were from Primer Design and had the following sequences: CATTGTGACTGAGGAAGAAGGA (Kir6.1, sense), GGTCTGAATAAGGATGGAAGGTT (antisense), GATGGTGGGAGGGACTGAG (Kir6.2, sense), and CAGAGTTCTAGGCAAGTTCACA (antisense). The efficiencies for the Kir6.x primers were not different (Kir6.1, Qiagen: 2.1±0.02; Kir6.2, Qiagen: 2.1±0.02; Kir6.1, Primer Design: 2.1±0.04; Kir6.2, Primer Design: 2.2±0.10). The primer sequences for SUR2A and SUR2B were as specified by Kajioka et al. (2011).

2.7. Immunoelectron microscopy

Strips were fixed (1.5% paraformaldehyde, 0.5% glutaraldehyde, in 0.1 M phosphate buffer, pH 7.4) for 1 h at room temperature, followed by washing with 0.1 M phosphate buffer, pH 7.4. The samples were subsequently dehydrated in ethanol and further processed for Lowicryl embedding (Carlemalm et al., 1985). Sections were cut and mounted on gold grids. For immunostaining, the grids were floated on top of drops of immune reagents dispensed on a sheet of parafilm. Free aldehyde groups were blocked with 50 mM glycine, and the grids were then incubated with 5% (v/v) goat serum in incubation buffer (0.2% acetylated bovine serum albumin in PBS (pH 7.6) for 15 min. This blocking procedure was followed by overnight incubation at 4 °C with M_3 receptor antibody (GTX13063, rabbit, 1:10, from GeneTex®, Inc., Shakirova et al., 2010a) and Kir6.1 antibody (sc-11224, goat, 1:10, Santa Cruz Biotechnology Inc., Sampson et al., 2007). Controls without primary antibodies were included. The grids were washed in a large volume (200 μl) of incubation buffer, floating on drops containing the gold conjugate reagents. 1 μg/ml anti-rabbit IgG 5 nm gold (BBI) and 1 μg/ml anti-goat IgG 20 nm gold were added, and the incubation was allowed to proceed for 2 h at 4 °C. After further washes, the sections were postfixed in 2% glutaraldehyde. Finally, sections were

washed with distilled water and post-stained with 2% uranyl acetate and lead citrate. Samples were examined with a JEOL JEM 1230 electron microscope operated at 80 kV accelerating voltage. Images were recorded with a Gatan Multiscan 791 charge-coupled device camera.

Three human bladder specimens were used for quantitative analysis of M_3 and Kir6.1 labeling. Ultrathin sections from different areas of the specimens were examined following the rules of systematic uniform random sampling. For each caveolae-containing plasma membrane stretch, the numbers of gold particles were counted and compared to non-specific background staining. A total of 50 cellular profiles were analyzed in each case.

2.8. Drugs and chemicals

Carbachol, glibenclamide, levcromacalim, chelerythrine and methyl-β-cyclodextrin were from Sigma. PNU-37883 (U37883A; 4-morpholinecarboximidine-N-1-adamantyl-N'-cyclohexyl-hydrochloride) and repaglinide were from Tocris. Vehicle (0.1% DMSO or 0.1% ethanol) was included in all control experiments (±mβcd).

2.9. Statistics

With the exception for mβcd + PNU-37883-treated preparations, a four parametric Hill equation was fitted to concentration-response data using the least squares method in order to retrieve the EC_{50} value. Student's t-test was used to test for significant differences. Bonferroni correction was used for multiple comparisons. $P<0.05$ was considered significant. In the figures *, ** and *** denote $P<0.05$, $P<0.01$, and $P<0.001$, respectively. For clarity, significant differences are not indicated in the concentration-response curves.

3. Results

3.1. Effect of mβcd on the ultrastructure of caveolae in human detrusor

Caveolae, clustered between dense bands (membrane-associated dense plaques), were numerous along the sarcolemma in control detrusor myocytes (**1A** and **B**). Schwann cells around detrusor nerves also contained caveolae (**1B**), but no caveolae were seen in neurons. After 1 and 2h of treatment with methyl-β-cyclodextrin (mβcd) caveolae in detrusor myocytes were flattened and dilated (**C**, **D**). The depths of 24 caveolae with visible necks were 90±3 nm (control), 69±4 nm (1 h mβcd), and 60±4 nm (2 h mβcd), while their opening diameters were 30±1 nm in controls, 59±3 nm at 1 h and 61±4 nm at 2 h (compare **1A**-**D**). Their maximal widths changed only marginally (69±2 nm, control; 67±2 nm, 1 h; 62±4 nm, 2 h).

3.2. Mechanical effects of mβcd

Few (87 out of 690 =13%) detrusor strips exhibited spontaneous contractile activity during equilibration. On treatment with mβcd following the reference contraction, a time-dependent shift to the right of the concentration-response curve for the muscarinic agonist carbachol was observed (**2A**, 3 strips from the same individual at each time). Consequently, the negative logarithm of the EC_{50} value for carbachol decreased (**2B**). Mβcd (1h, n=5) did not reduce K^+-induced contraction at any K^+ concentration between 10 and 50 mM (**2C**). When cholesterol was reloaded after 1h treatment with mβcd, the concentration response relationship for carbachol was shifted back left (**2D**, n=6). While reloading of cholesterol led to a slight reduction of the E_{max} value, contractility was fully restored at carbachol concentrations below 1 μM (**2E**), and the EC_{50} value recovered completely (**2F**). Thus, the mechanical effects of

mβcd are time-dependent, correlate with ultrastructural effects on caveolae, are specific for receptor-induced contractions, and depend largely on removal of cholesterol.

3.3. Effects of drugs that target K_{ATP} channels

An increased extracellular K^+ concentration should reduce the driving force for an outward K^+ current. We contracted detrusor preparations partially using 25 mM K^+ and then added carbachol in a cumulative manner. Under these conditions cholesterol desorption did not inhibit muscarinic contractility (**3A**, n=6). In control strips, from the same patients and run in parallel, a clear-cut inhibition was seen (effect at 0.1 μM carbachol is shown in **3B**).

To test the involvement of K_{ATP} channels, the rightward shift of the concentration response curve in the absence (**3C**) and presence (**3D**) of the K_{ATP} current inhibitor glibenclamide (10 μM) was compared. Mβcd increased the EC_{50} value 2.6±0.4-fold in control conditions and 1.5±0.1-fold in the presence of glibenclamide (10 μM, $P<0.05$, n=6, **3E**). Similarly, no significant right shift was induced by mβcd in the presence of the K_{ATP} inhibitor repaglinide (10 μM, n=6, $P>0.05$ for the effect of mβcd). Incubation with the K_{ATP} activator levcromakalim (1 μM, **3F**) mimicked the effect of mβcd and caused a 3.9±0.4-fold shift to the right of the concentration-response curve (n=6, **3G**). Thus, the effect of mβcd on cholinergic detrusor activation is inhibited by K_{ATP} channel blockers and mimicked by K_{ATP} channel activation.

3.4. PNU-37883 reverses the effect of cholesterol desorption in human bladder

Kir6.1 is a candidate pore component of the human bladder K_{ATP} channel. To test its role in the effect of cholesterol desorption we used the Kir6.1 blocker PNU37883. This substance (at 20 μM) had a pronounced effect after desorption of cholesterol (**4B** vs. **4A**); at submaximal concentrations of carbachol, force was increased ($P<0.05$ at 0.1 μM carbachol) rather than decreased, and the concentration-response curve exhibited two apparent phases (**4B**). No rightward shift was seen in the presence of PNU37883 whereas a 2.7±0.4-fold rightward shift was induced by mβcd in the matched control preparations from the same individuals (**4C**, n=6). We also tested the reverse experiment, i.e. adding PNU37883 to control and mβcd-treated preparations after having increased the carbachol concentration cumulatively to 0.1 μM. As expected, control strips contracted transiently to about 40% of the reference contraction at this concentration whereas the mβcd treated strips contracted little (**4D**). On addition of PNU37883, control strips continued to relax after the transient response to carbachol (**4D**, four out of four strips) whereas a sustained contraction was elicited in four out of four mβcd-treated strips.

3.5. Probing the composition of K_{ATP} channel in human urinary bladder using RT-qPCR

Because our mechanical experiments suggested involvement of K_{ATP} channels and Kir6.1 in the effect of cholesterol desorption in human bladder, we examined expression of K_{ATP} channel subunits using RT-qPCR. Kir6.x primer efficiencies were comparable, and using two different primer pairs for each target, it was clear that Kir6.1 expression dominated over Kir6.2 (**5A**). We were unable to achieve a quantitative comparison of sulphonylurea receptor

expression, but products of expected sizes were seen using SUR1, pan-SUR2, and SUR2B primers (**5B**).

3.6. Detection of Kir6.1 by Western blotting and co-fractionation with M_3 and caveolin-1

In keeping with Kir6.1 mRNA expression in human bladder, the protein product was detected by Western blotting (**6A**). Mouse aorta was included as positive control. To probe the subcellular distribution of Kir6.1 and muscarinic M_3 receptors we used sucrose density fractionation (n=4). Caveolin-1 was primarily distributed in fractions 5-8 with a peak in fractions 5-6 (**6B**). M_3 and Kir6.1 similarly showed a broad distribution with a peak in fraction 6 (**6B**). The cytoskeletal protein SM22α was present in the high density fractions, as was the majority of cellular protein (not shown).These findings are consistent with the possibility that M_3 and Kir6.1 reside in caveolae.

3.7. Immunoelectron microscopy shows co-localization of M_3 and Kir6.1 in caveolae

Kir6.1and M_3 were next labeled with immunogold. Figure **7A** shows an overview acquired by conventional electron microscopy using the same detrusor as in panels **B** and **C**. Panels **B** and **C** show immunogold labeling of M_3 (5 nm gold) and Kir6.1 (20 nm gold). Both proteins were enriched in caveolae with less labeling of planar membrane (**7B** and **C**). Clusters of submembranous caveolae were also labeled, and vesicles with gold particles were occasionally observed deeper in the cytoplasm. Panels **D** and **E** show M_3 and Kir6.1 distribution in two additional individuals.

The total number of small gold particles (M_3) counted was 1549, 1898 and 1721, and the number of large gold particles (Kir6.1) was 581, 629, and 601, respectively. Of these, 1177 (76%), 1480 (78%) and 1256 (73%) small gold particles, and 604 (71%), 434 (69%) and 421

(70%) large gold particles were localized to caveolae. Thus, ~70% of both Kir6.1 and M_3 is confined to caveolae, which constitute ~28% of the membrane surface length. M_3 and Kir6.1 are therefore enriched 6-fold in caveolae.

3.8. Chelerythrine inhibits the rightward shift of the concentration-response curve for carbachol

Co-localization of M_3 and Kir6.1 in caveolae may be a prerequisite for M_3-mediated inhibition of Kir6.1. Indeed, the PKC translocation inhibitor chelerythrine (3 μM) effectively inhibited the rightward shift induced by mβcd (1.6±0.2-fold with chelerythrine vs. 3.9±0.6-fold in the controls, n=6, Figure **8A-C**). However, chelerythrine had no effect in control conditions (**8D**).

4. Discussion

We present ultrastructural evidence favoring a caveolar localization of M_3 receptors and Kir6.1-containing K_{ATP} channels in the human detrusor. We moreover show that three different K_{ATP} channel blockers, representing different structural classes and with non-overlapping off-target effects, antagonize the effects of caveolae disruption on muscarinic detrusor activation. Findings with chelerythrine moreover suggest that protein kinase C is involved in the effect of cholesterol desorption.

Muscarinic receptor-mediated and protein kinase C-dependent inhibition of K_{ATP} current has been demonstrated in guinea pig detrusor (Bonev and Nelson, 1993). One possibility therefore is that colocalization of M_3 receptors and K_{ATP} channels in caveolae facilitate inhibition of the channels as a component of the excitatory influence of muscarinic stimulation. A restricted inhibition of K_{ATP} channels within caveolae implies the presence of a caveolar "signalosome". Indeed, $G_{\alpha q}$ (Oh and Schnitzer, 2001), phospholipase $C_{\beta 1}$ (Sharma et al., 2010), and protein kinase C (Mineo et al., 1998, Sampson et al., 2007), have been demonstrated to associate with caveolae in a static or dynamic manner in other cells and tissues. Our findings with the protein kinase C inhibitor chelerythrine, which is known to mitigate receptor-induced K_{ATP} current inhibition (Thorneloe et al., 2002), are however not entirely consistent with this possibility. While chelerythrine inhibited the effect of mβcd on muscarinic contraction, it had little effect on the muscarinic contraction as such.

Our present and previous (Shakirova et al., 2010a) data on the effects of cholesterol desorption in the human bladder do not support loss of M_3 receptors, reduced ligand binding to M_3 receptors, or a generalized impairment of M_3 receptor coupling. Treatment with either 25 mM K^+ or PNU-37883, a Kir6.1 channel blocker (Surah-Narwal et al., 1999), completely

antagonized the effect of cholesterol desorption. This would not occur if desorption of cholesterol had a major effect on ligand binding or on the contractile machinery. Similar conclusions were reached by Gosens et al. (2007) on the basis of ligand binding assays using airway smooth muscle cells.

We find that Kir6.1 is expressed in human detrusor. This confirms work on Kir6.x mRNA expression in commercial human bladder RNA preparations (Kajioka et al., 2011). Similarly, SUR2B was readily detectable. It is therefore reasonable to infer that Kir6.1/SUR2B containing K_{ATP} channels are present, if not dominating, in human detrusor myocytes, which implies regulation by caveolin-1/caveolae similar to that seen in HEK293 cells (Davies et al., 2010).

Disruption of caveolae has little effect on muscarinic contraction in some species (Shakirova et al., 2006, 2010a, 2010b). A difference in regulation depending on the molecular make-up of the K_{ATP} channel is one putative reason for this. Indeed, substantial differences in the effect of drugs that target K_{ATP} channels exist between man and rodent bladders (Wammack et al., 1994). Interestingly, caveolin-1 levels drop in human detrusor hypertrophy associated with benign prostatic hyperplasia (Boopathi et al., 2011). This could result in altered excitability via K_{ATP} channels.

In conclusion, our pharmacological findings suggest that protein kinase C and K_{ATP} channels are involved in the effect of cholesterol desorption, which disrupts caveolae, on muscarinic contraction in the human detrusor. M_3 receptors and Kir6.1 moreover localize to detrusor caveolae. To the best of our knowledge, no previous description has been provided of the ultrastructural localization of these important signaling proteins in the human bladder.

Acknowledgements

Supported by grants from the Swedish Research Council (K2009-65X-4955-01-3, K2011-67P-20608-02-4), ALF, the Crafoord Foundation, the Hillevie Fries Foundation, and the Faculty of Medicine at Lund University. KS holds a Researcher position at the Swedish Research Council. We thank Rita Wallén, Lina Gefors, and Maria Baumgarten for expert assistance with electron microscopy.

REFERENCES

Aishima, M., Tomoda, T., Yunoki, T., Nakano, T., Seki, N., Yonemitsu, Y., Sueishi, K., Naito, S., Ito, Y., Teramoto, N., 2006. Actions of ZD0947, a novel ATP-sensitive K^+ channel opener, on membrane currents in human detrusor myocytes. Br. J. Pharmacol. 149, 542-550.

Andersson, K.E., 2011. Muscarinic acetylcholine receptors in the urinary tract. Handb. Exp. Pharmacol. 202, 319-344.

Bastiani, M., Liu, L., Hill, M.M., Jedrychowski, M.P., Nixon, S.J., Lo, H.P., Abankwa, D., Luetterforst, R., Fernandez-Rojo, M., Breen, M.R., Gygi, S.P., Vinten, J., Walser, P.J., North, K.N., Hancock, J.F., Pilch, P.F., Parton, R.G., 2009. MURC/Cavin-4 and cavin family members form tissue-specific caveolar complexes. J. Cell. Biol. 185, 1259-1273.

Bonev, A.D., Nelson, M.T., 1993. Muscarinic inhibition of ATP-sensitive K^+ channels by protein kinase C in urinary bladder smooth muscle. Am. J. Physiol. 265, C1723-C1728.

Boopathi, E., Gomes, C.M., Goldfarb, R., John, M., Srinivasan, V.G., Alanzi, J., Malkowicz, S.B., Kathuria, H., Zderic, S.A., Wein, A.J., Chacko, S., 2011. Transcriptional Repression of Caveolin-1 (CAV1) Gene Expression by GATA-6 in Bladder Smooth Muscle Hypertrophy in Mice and Human Beings. Am. J. Pathol. 178, 2236-2251.

Carlemalm, E., Villiger, W., Hobot, J.A., Acetarin, J.D., Kellenberger, E., 1985. Low temperature embedding with Lowicryl resins: two new formulations and some applications. J. Microsc. 140, 55–63.

Chang, W.J., Ying, Y.S., Rothberg, K.G., Hooper, N.M., Turner, A.J., Gambliel, H.A., De Gunzburg, J., Mumby, S.M., Gilman, A.G., Anderson, R.G., 1994. Purification and characterization of smooth muscle cell caveolae. J. Cell. Biol. 126, 127-138.

Chun, M., Liyanage, U.K., Lisanti, M.P., Lodish, H.F., 1994. Signal transduction of a G protein-coupled receptor in caveolae: colocalization of endothelin and its receptor with caveolin. Proc. Natl. Acad. Sci. 91, 11728-11732.

Cohen, A.W., Hnasko, R., Schubert, W., Lisanti, M.P., 2004. Role of caveolae and caveolins in health and disease. Physiol. Rev. 84, 1341-1379.

Davies, L.M., Purves, G.I., Barrett-Jolley, R., Dart, C., 2010. Interaction with caveolin-1 modulates vascular ATP-sensitive potassium (K_{ATP}) channel activity. J. Physiol. 588, 3255-3266.

Dreja, K., Voldstedlund, M., Vinten, J., Tranum-Jensen, J., Hellstrand, P., Swärd, K., 2002. Cholesterol depletion disrupts caveolae and differentially impairs agonist-induced arterial contraction. Arterioscler. Thromb. Vasc. Biol. 22, 1267-1272.

Fry, C.H., Meng, E., Young, J.S., 2010. The physiological function of lower urinary tract smooth muscle. Auton. Neurosci. 154, 3-13.

Fujita, A., Cheng, J., Tauchi-Sato, K., Takenawa, T., Fujimoto, T., 2009. A distinct pool of phosphatidylinositol 4,5-bisphosphate in caveolae revealed by a nanoscale labeling technique. Proc. Natl. Acad. Sci. 106, 9256-9261.

Gabella, G., 1976. Quantitative morphological study of smooth muscle cells of the guinea-pig taenia coli. Cell. Tissue. Res. 170, 161-186.

Gabella, G., Blundell, D., 1978. Effect of stretch and contraction on caveolae of smooth muscle cells. Cell. Tissue. Res. 190, 255-271.

Gosens, R., Stelmack, G.L., Dueck, G., Mutawe, M.M., Hinton, M., McNeill, K.D., Paulson, A., Dakshinamurti, S., Gerthoffer, W.T., Thliveris, J.A., Unruh, H., Zaagsma, J., Halayko, A.J., 2007. Caveolae facilitate muscarinic receptor-mediated intracellular Ca^{2+} mobilization and contraction in airway smooth muscle. Am. J. Physiol. Lung Cell. Mol. Physiol. 293, L1406-1418.

Hill, M.M., Bastiani, M., Luetterforst, R., Kirkham, M., Kirkham, A., Nixon, S.J., Walser, P., Abankwa, D., Oorschot, V.M., Martin, S., Hancock, J.F., Parton, R.G., 2008. PTRF-Cavin, a conserved cytoplasmic protein required for caveola formation and function. Cell 132, 113-124.

Kajioka, S., Shahab, N., Asano, H., Morita, H., Sugihara, M., Takahashi-Yanaga, F., Yoshihara, T., Nakayama, S., Seki, N., Naito, S., 2011. Diphosphate Regulation of Adenosine Triphosphate Sensitive Potassium Channel in Human Bladder Smooth Muscle Cells. J Urol. 186, 736-44.

Lai, H.H., Boone, T.B., Yang, G., Smith, C.P., Kiss, S., Thompson, T.C., Somogyi, G.T., 2004. Loss of caveolin-1 expression is associated with disruption of muscarinic cholinergic activities in the urinary bladder. Neurochem. Int. 45, 1185-1193.

Lisanti, M.P., Scherer, P.E., Tang, Z., Sargiacomo, M., 1994. Caveolae, caveolin and caveolin-rich membrane domains: a signalling hypothesis. Trends Cell Biol. 4, 231-235.

Matsui, M., Motomura, D., Karasawa, H., Fujikawa, T., Jiang, J., Komiya, Y., Takahashi, S., Taketo, M.M., 2000. Multiple functional defects in peripheral autonomic organs in mice lacking muscarinic acetylcholine receptor gene for the M_3 subtype. Proc. Natl. Acad. Sci. 97, 9579-9584.

Mineo, C., Ying, Y.S., Chapline, C., Jaken, S., Anderson, R.G., 1998. Targeting of protein kinase Calpha to caveolae. J Cell Biol. 141, 601-610.

North, A.J., Galazkiewicz, B., Byers, T.J., Glenney, J.R. Jr, Small, J.V., 1993. Complementary distributions of vinculin and dystrophin define two distinct sarcolemma domains in smooth muscle. J. Cell. Biol. 120, 1159-1167.

Oh, P., Schnitzer, J.E. 2001., Segregation of heterotrimeric G proteins in cell surface microdomains. G(q) binds caveolin to concentrate in caveolae, whereas G(i) and G(s) target lipid rafts by default. Mol Biol Cell. 12, 685-698.

Rothberg, K.G., Heuser, J.E., Donzell, W.C., Ying, Y.S., Glenney, J.R., Anderson, R.G., 1992. Caveolin, a protein component of caveolae membrane coats. Cell 68, 673-682.

Sadegh, M.K., Ekman, M., Rippe, C., Sundler, F., Wierup, N., Mori, M., Uvelius, B., Swärd, K., 2011. Biomechanical properties and innervation of the female caveolin-1-deficient detrusor. Br. J. Pharmacol. 162, 1156-1170.

Sampson, L.J., Hayabuchi, Y., Standen, N.B., Dart, C., 2004. Caveolae localize protein kinase A signaling to arterial ATP-sensitive potassium channels. Circ. Res. 95, 1012-1018.

Sampson, L.J., Davies, L.M., Barrett-Jolley, R., Standen, N.B., Dart, C., 2007. Angiotensin II-activated protein kinase C targets caveolae to inhibit aortic ATP-sensitive potassium channels. Cardiovasc. Res. 76, 61-70.

Shakirova, Y., Bonnevier, J., Albinsson, S., Adner, M., Rippe, B., Broman, J., Arner, A., Swärd, K., 2006. Increased Rho activation and PKC-mediated smooth muscle contractility in the absence of caveolin-1. Am. J. Physiol. Cell Physiol. 291, C1326-1335.

Shakirova, Y., Mori, M., Ekman, M., Erjefält, J., Uvelius, B., Swärd, K., 2010a. Human urinary bladder smooth muscle is dependent on membrane cholesterol for cholinergic activation. Eur. J. Pharmacol. 634, 142-148.

Shakirova, Y., Swärd, K., Uvelius, B., Ekman, M., 2010b. Biochemical and functional correlates of an increased membrane density of caveolae in hypertrophic rat urinary bladder. Eur. J. Pharmacol. 649, 362-368.

Sharma, P., Ghavami, S., Stelmack, G.L., McNeill, K.D., Mutawe, M.M., Klonisch, T., Unruh, H., Halayko, A.J., 2010. β-Dystroglycan binds caveolin-1 in smooth muscle: a functional role in caveolae distribution and Ca^{2+} release. J. Cell Sci. 123, 3061-3070.

Shaul, P.W., Anderson, R.G., 1998. Role of plasmalemmal caveolae in signal transduction. Am. J. Physiol. 275: L843-851.

Surah-Narwal, S., Xu, S.Z., McHugh, D., McDonald, R.L., Hough, E., Cheong, A., Partridge, C., Sivaprasadarao, A., Beech, D.J., 1999. Block of human aorta Kir6.1 by the vascular K_{ATP} channel inhibitor U37883A. Br. J. Pharmacol. 128, 667-672.

Thorneloe, K.S., Maruyama, Y., Malcolm, A.T., Light, P.E., Walsh, M.P., Cole, W.C., 2002. Protein kinase C modulation of recombinant ATP-sensitive K^+ channels composed of Kir6.1 and/or Kir6.2 expressed with SUR2B. J. Physiol. 541, 65-80.

Wammack, R., Jahnel, U., Nawrath, H., Hohenfellner, R., 1994. Mechanical and electrophysiological effects of cromakalim on the human urinary bladder. Eur. Urol. 26, 176-181.

Woodman, S.E., Cheung, M.W., Tarr, M., North, A.C., Schubert, W., Lagaud, G., Marks, C.B., Russell, R.G., Hassan, G.S., Factor, S.M., Christ, G.J., Lisanti, M.P., 2004. Urogenital alterations in aged male caveolin-1 knockout mice. J. Urol. 171, 950-957.

Legends

Figure 1. Desorption of cholesterol using methyl-β-cyclodextrin (mβcd) causes a time-dependent deterioration of human detrusor caveolae. Human bladder preparations were incubated in HEPES-buffered Krebs buffer alone (**A** and **B**) or in 10 mM mβcd dissolved in the same buffer for one (**C**) and two (**D**) hours, respectively. In control conditions, caveolae (highlighted with arrowheads) were numerous (**A**). Caveolae were also seen in Schwann cells wrapped around detrusor nerves (**B**, center structure), but not in neurons. After desorption of cholesterol, caveolae were shallower with an increased neck-to-width ratio (**C**, **D**). After 1h normal appearing caveolae were still present in some regions (inset in **C**). At 2h a more complete change was apparent (arrowheads in **D**). All panels were acquired at 60K magnification and the scale bars represent 0.5 μm.

Figure 2. Desorption of cholesterol induces a rightward shift of the concentration-response curve for carbachol (Cch) in human detrusor. Cumulative concentration-response curves were generated using the muscarinic agonist carbachol at time 0 and after 1, 2, and 3 h of cholesterol desorption (**A**, means of three strips from one individual are shown, i.e. n=1). Force was normalized to the reference, K^+-high (60 mM; HK), contraction at the start of the experiment. Desorption of cholesterol time-dependently reduced the negative logarithm of the EC_{50} value for carbachol (**B**). Contraction induced by cumulative addition of K^+ was unaffected by mβcd (1h, n=5, **C**). Reloading of cholesterol reversed the effect of mβcd (1h) on carbachol contraction at low to intermediate carbachol concentrations (n=6, **D**). **E** shows force at 0.1 μM carbachol from the experiment in **D**. **F** shows potency (-log (EC_{50})) from experiment in **D**.

Figure 3. Effect of KCl and K_{ATP} channel inhibition on the effect of cholesterol desorption in the human detrusor. Panel **A** shows force in control and mβcd-treated human detrusor strips when 25 mM KCl was added just prior to the cumulative addition of carbachol. **B** shows force at 0.1 μM carbachol from experiment in **A**. **C** and **D** show concentration response curves for carbachol from the same individuals (n=6) in the absence (**C**) and presence of glibenclamide. Cholesterol desorption for 1h caused a 2.6-fold right shift of the concentration-response curve for carbachol and K_{ATP} current blocker glibenclamide (10 μM) reduced this effect (**E**). The dotted line in **E** represents the fold shift of the concentration response curve with 25 mM KCl in the solution. Levcromakalim (1 μM), a K_{ATP} channel activator, mimicked the effect of cholesterol desorption (**F** and **G**, n=6).

Figure 4. The Kir6.1 blocker PNU37883 (U37883A) reverses the effect of cholesterol desorption in the human detrusor. Vehicle-treated (± mβcd, **A**) and PNU37883-treated (20 μM, ± mβcd, **B**) preparations from the same patients were run in parallel. Open circles represent mβcd treated strips. **C** shows the fold shift induced by mβcd in the absence and presence of PNU37883 (n=6). **D** shows an original record of force where PNU37883 was added to a control (thick trace) and an mβcd-treated (thin trace) preparation after increasing the carbachol concentration in a step-wise fashion to 0.1 μM (4 preparations from one individual). The dotted line represents basal force. Responses elicited by low and intermediate concentrations were typically transient.

Figure 5. RT-qPCR showing that Kir6.1 mRNA level exceeds Kir6.2 mRNA level in human detrusor (**A**, n=10-12). Two different primer pairs for each target were used and each primer pair is represented by a bar. Sulphonylurea receptor expression is shown in **B** (n=6). Examples from two individuals are shown.

Figure 6. Detection of Kir6.1 by Western blotting and co-fractionation of muscarinic M_3 receptors and Kir6.1 with caveolin-1. Human detrusor and mouse aortic lysates were loaded on SDS-PAGE gels and Kir6.1 was detected by Western blotting (**A**). The amount of protein loaded is indicated below each lane. Bands are from the same blot, but four lanes were excised and omitted (indicated by the central vertical line). Blotting of sucrose gradient fractions (1-12) showing distribution of caveolin-1, M_3 receptors, Kir6.1, and the actin binding protein SM22α (**B**, n=4).

Figure 7. Immunoelectron microscopy demonstrates co-localization of muscarinic M_3 (5 nm gold) receptors and Kir6.1 (20 nm gold) in caveolae of human detrusor smooth muscle cells. Panel **A** shows an overview by conventional electron microscopy of the same bladder that was used for labeling in **B** and **C**. Caveolae are highlighted with arrow heads. Panel **B** is focused on flat membrane and panel **C** on a cluster of caveolae in the lower cell. Note that the caveolae-free membrane segment in the upper cell essentially is devoid of labeling. Panels **D** and **E** show localization of M_3 and Kir6.1 in two additional bladders. The scale bars in **A** and **E** represent 0.5 and 0.1 μm, respectively. The latter scale bar applies for panels **B** through **E**.

Figure 8. Chelerythrine, a protein kinase C translocation inhibitor, largely eliminates the rightward shift of the concentration-response relationship that is induced by cholesterol desorption in human detrusor. **A** and **B** show the effect of mβcd in control preparations and in the presence of chelerythrine, respectively. **C** shows the fold shift induced by mβcd in the absence and presence of chelerythrine (3 μM, n=6 for both).

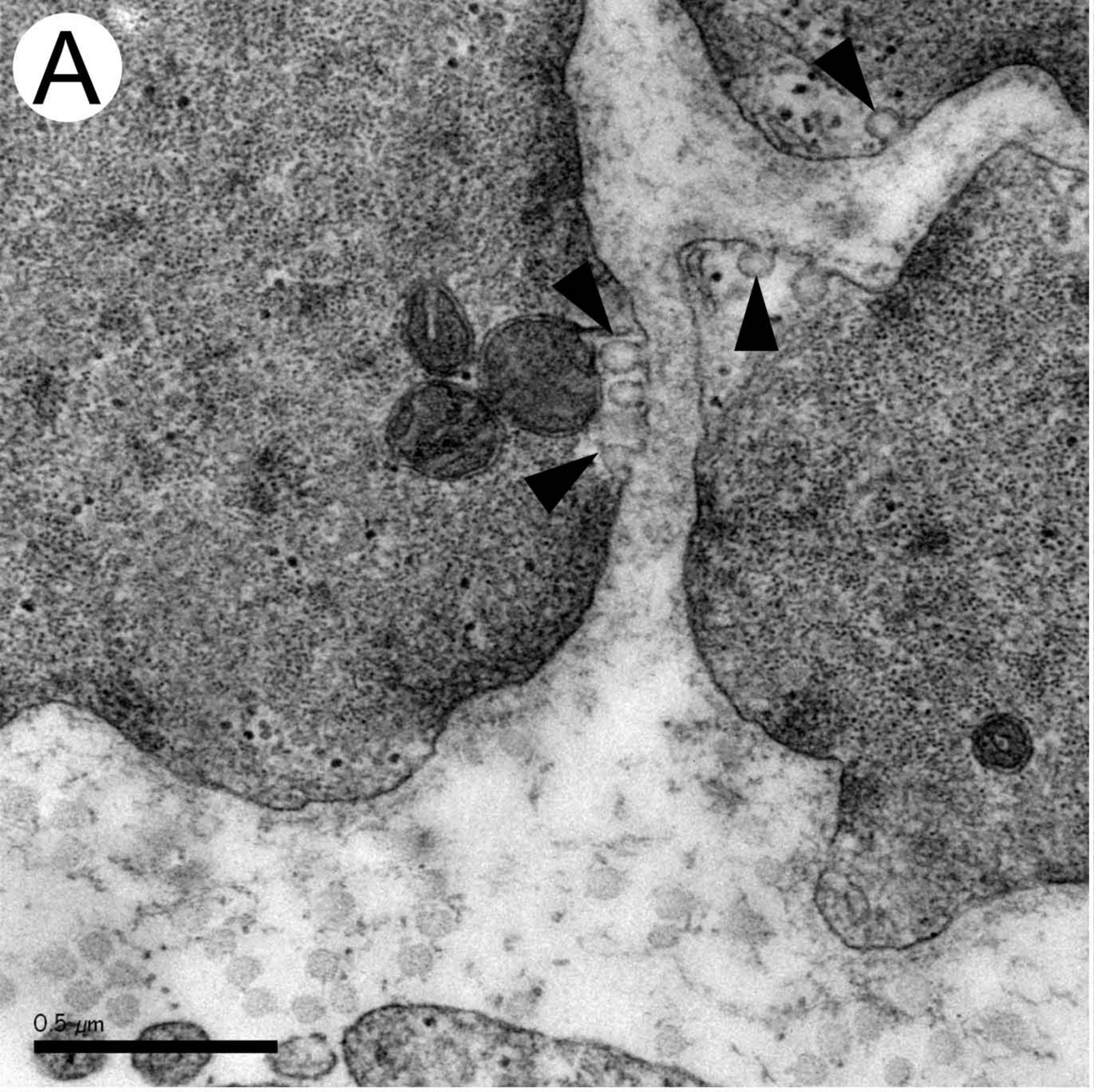
A
0.5 μm

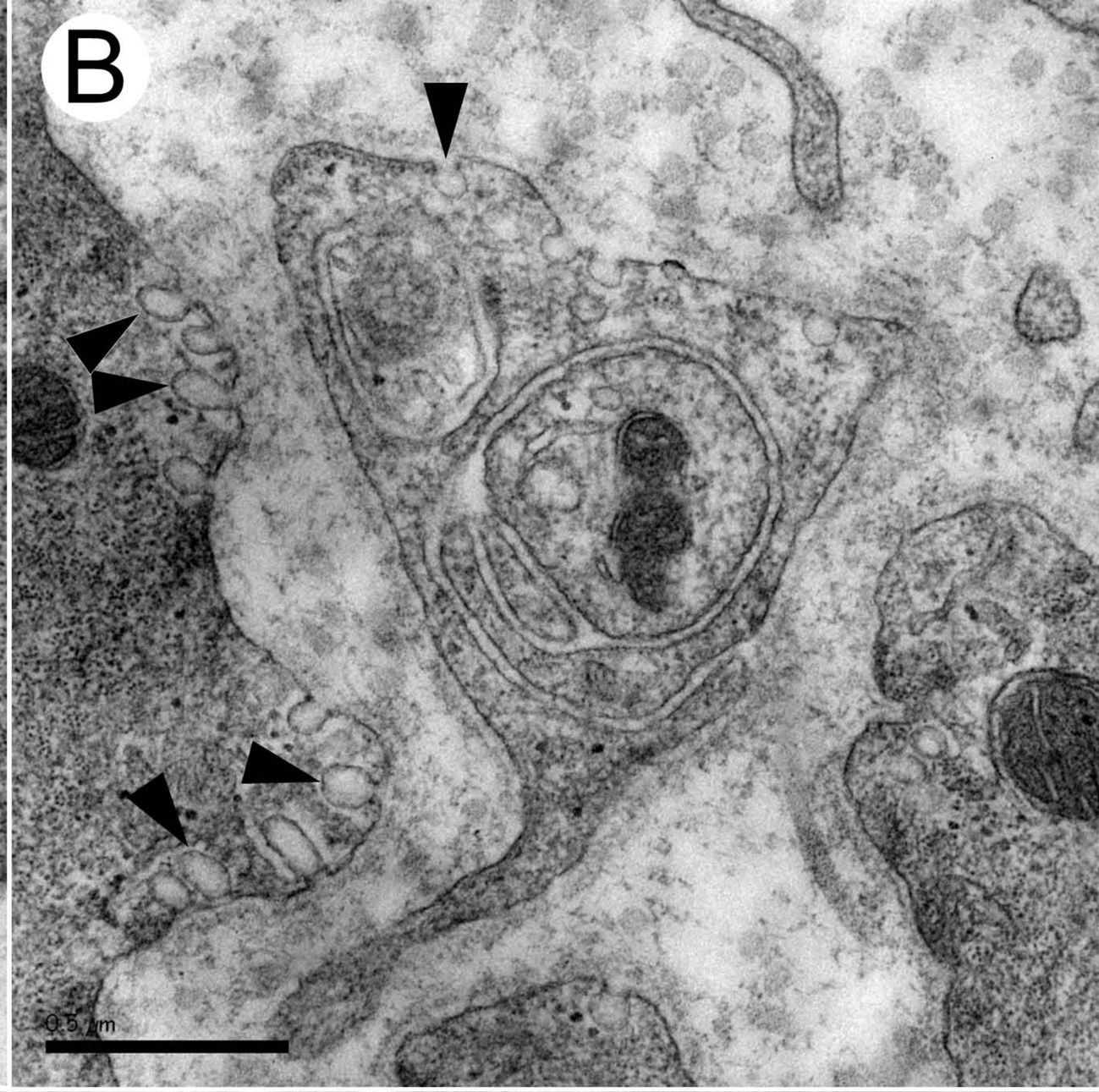
B
0.5 μm

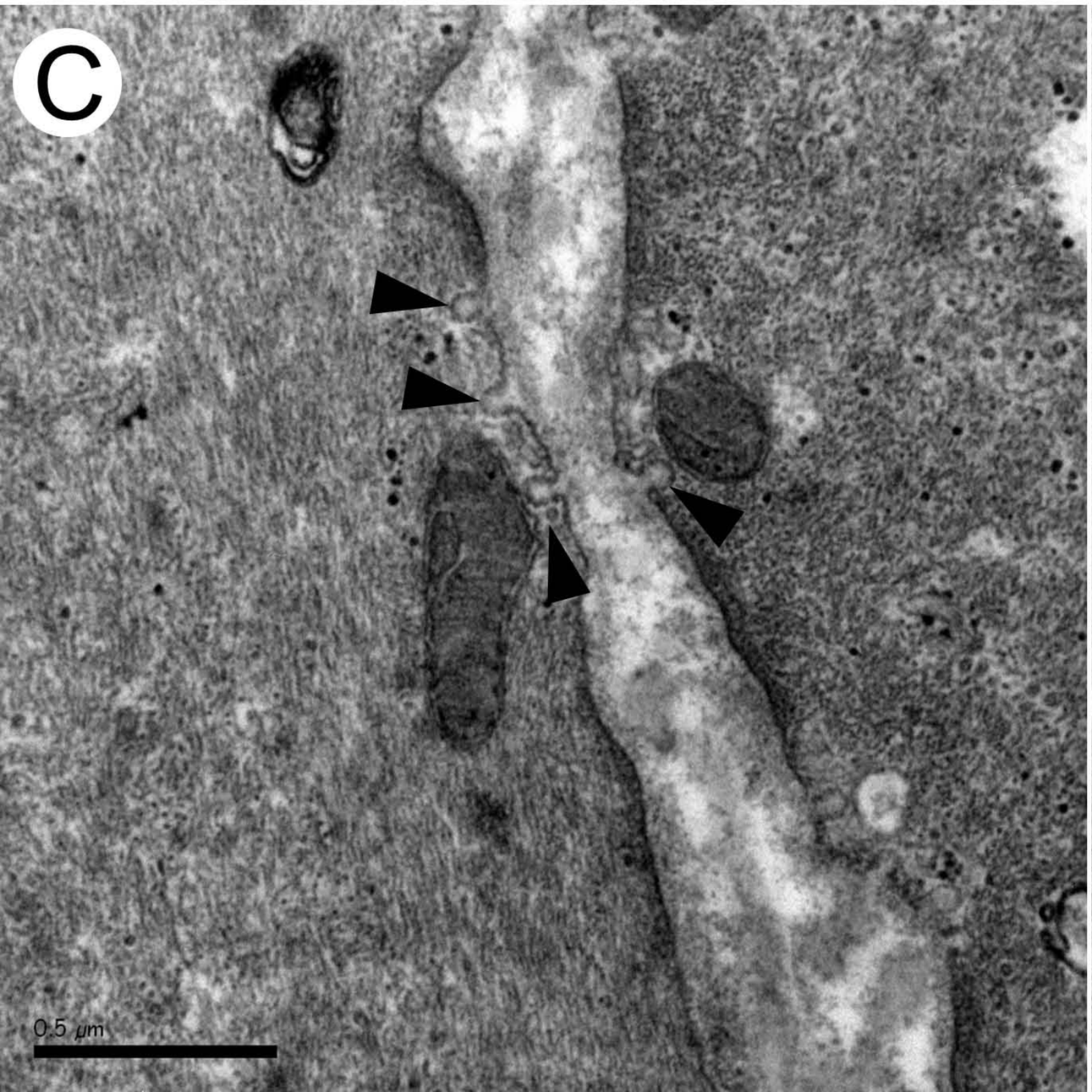
C
0.5 μm

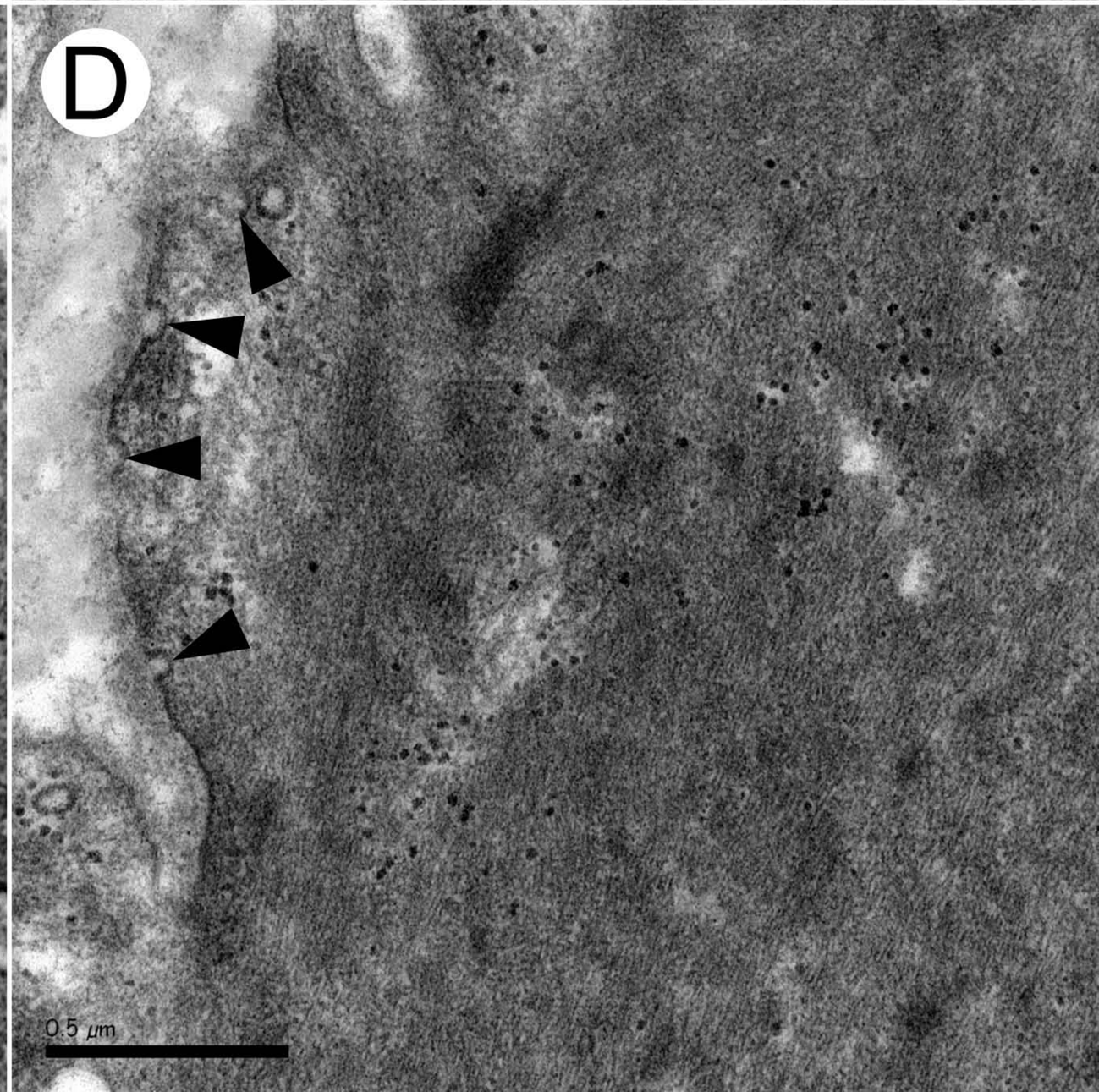
D
0.5 μm

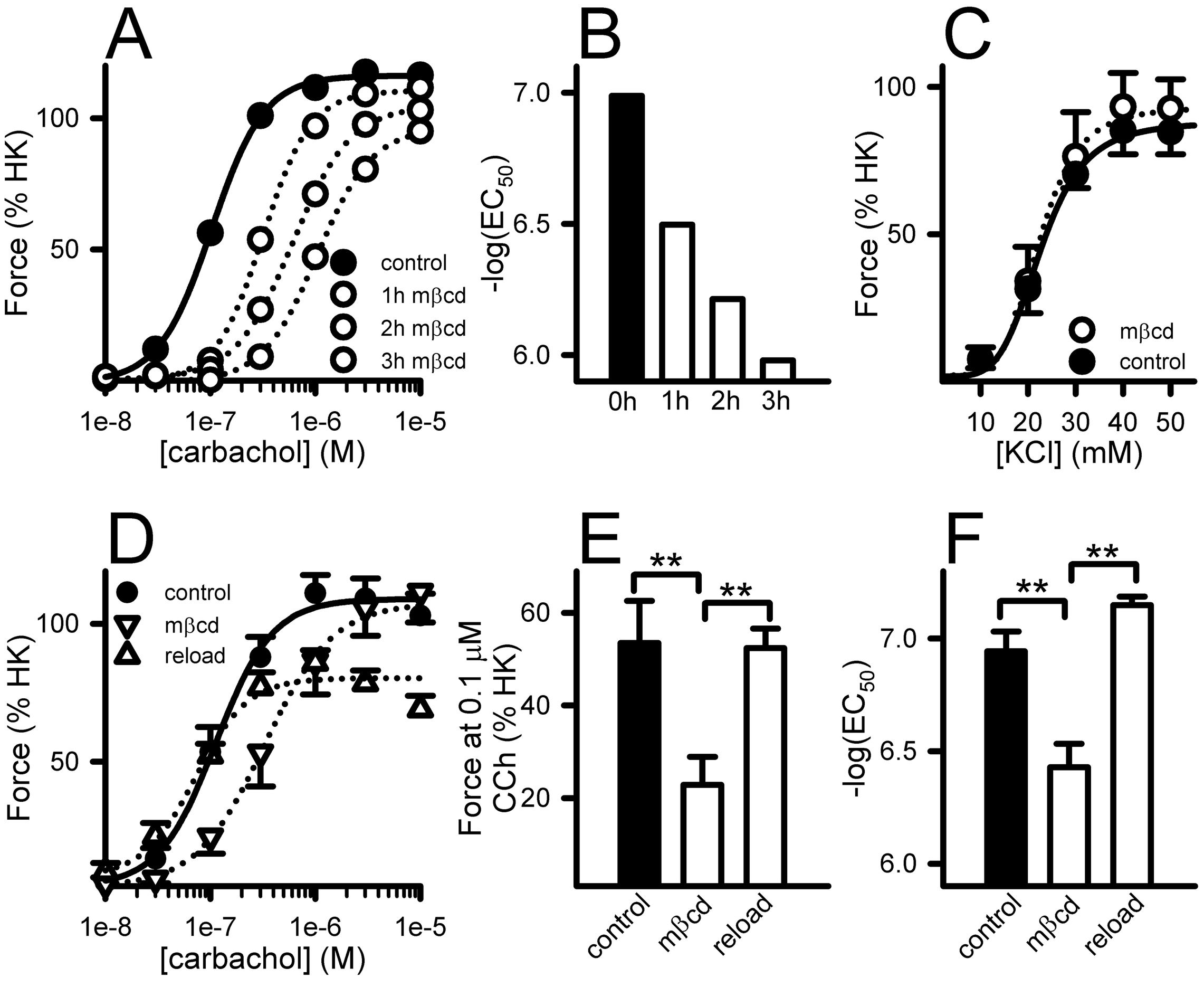
A
Force (% HK)
100
50
control
1h mβcd
2h mβcd
3h mβcd
1e-8
1e-7
1e-6
1e-5
[carbachol] (M)
B
-log(EC50)
7.0
6.5
6.0
0h
1h
2h
3h
C
Force (% HK)
100
50
mβcd
control
10
20
30
40
50
[KCl] (mM)
D
control
mβcd
reload
Force (% HK)
100
50
1e-8
1e-7
1e-6
1e-5
[carbachol] (M)
E
**
**
Force at 0.1 μM CCh (% HK)
60
40
20
control
mβcd
reload
F
**
**
-log(EC50)
7.0
6.5
6.0
control
mβcd
reload

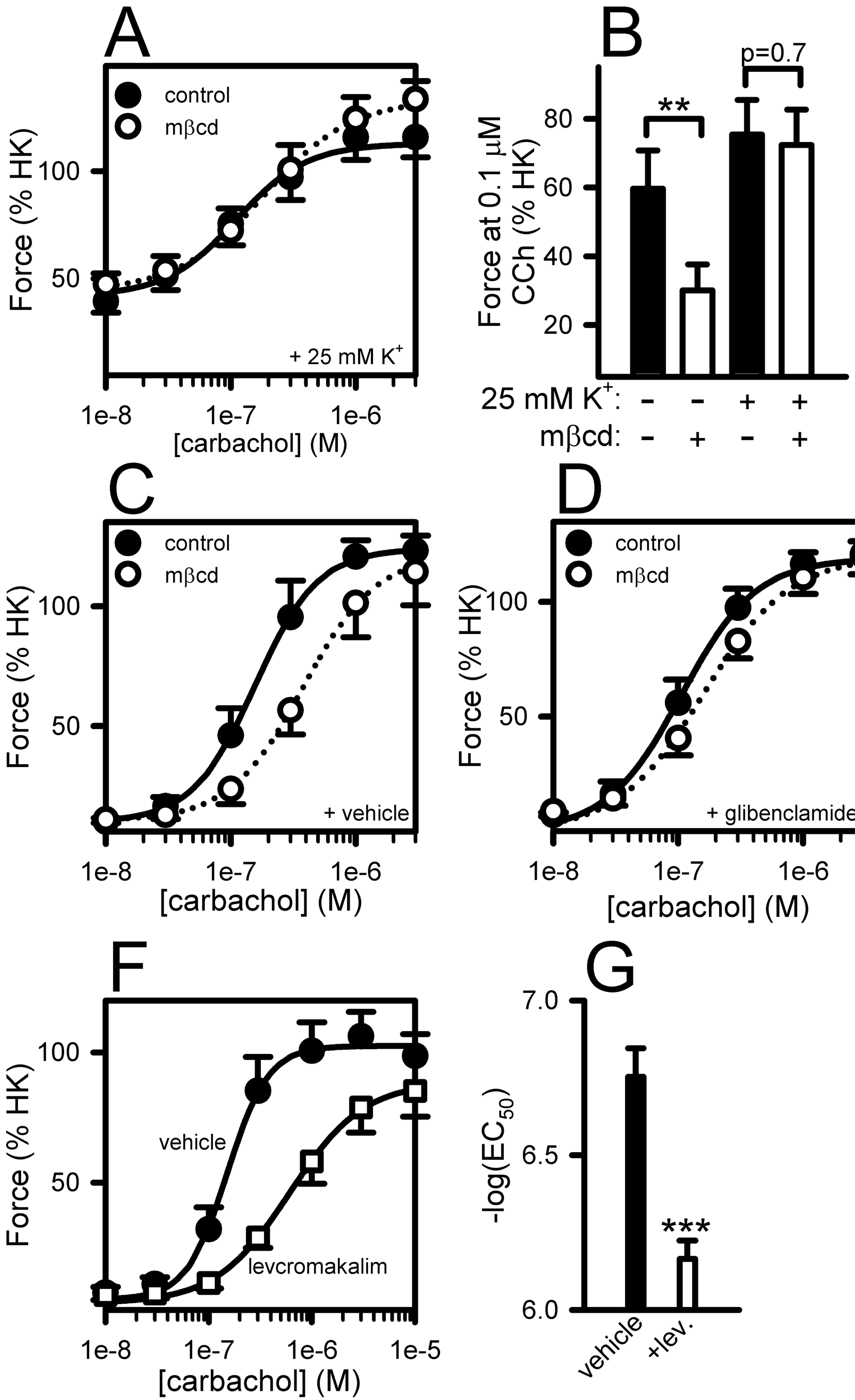
A
control
mβcd
+ 25 mM K+
Force (% HK)
100
50
1e-8
1e-7
1e-6
[carbachol] (M)
B
p=0.7
**
Force at 0.1 μM CCh (% HK)
80
60
40
20
25 mM K+: - - + +
mβcd: - + - +
C
control
mβcd
+ vehicle
Force (% HK)
100
50
1e-8
1e-7
1e-6
[carbachol] (M)
D
control
mβcd
+ glibenclamide
Force (% HK)
100
50
1e-8
1e-7
1e-6
[carbachol] (M)
E
EC50+mβcd/EC50-mβcd
3
2
1
0
*
vehicle
+glib.
F
vehicle
levcromakalim
Force (% HK)
100
50
1e-8
1e-7
1e-6
1e-5
[carbachol] (M)
G
-log(EC50)
7.0
6.5
6.0
***
vehicle
+lev.

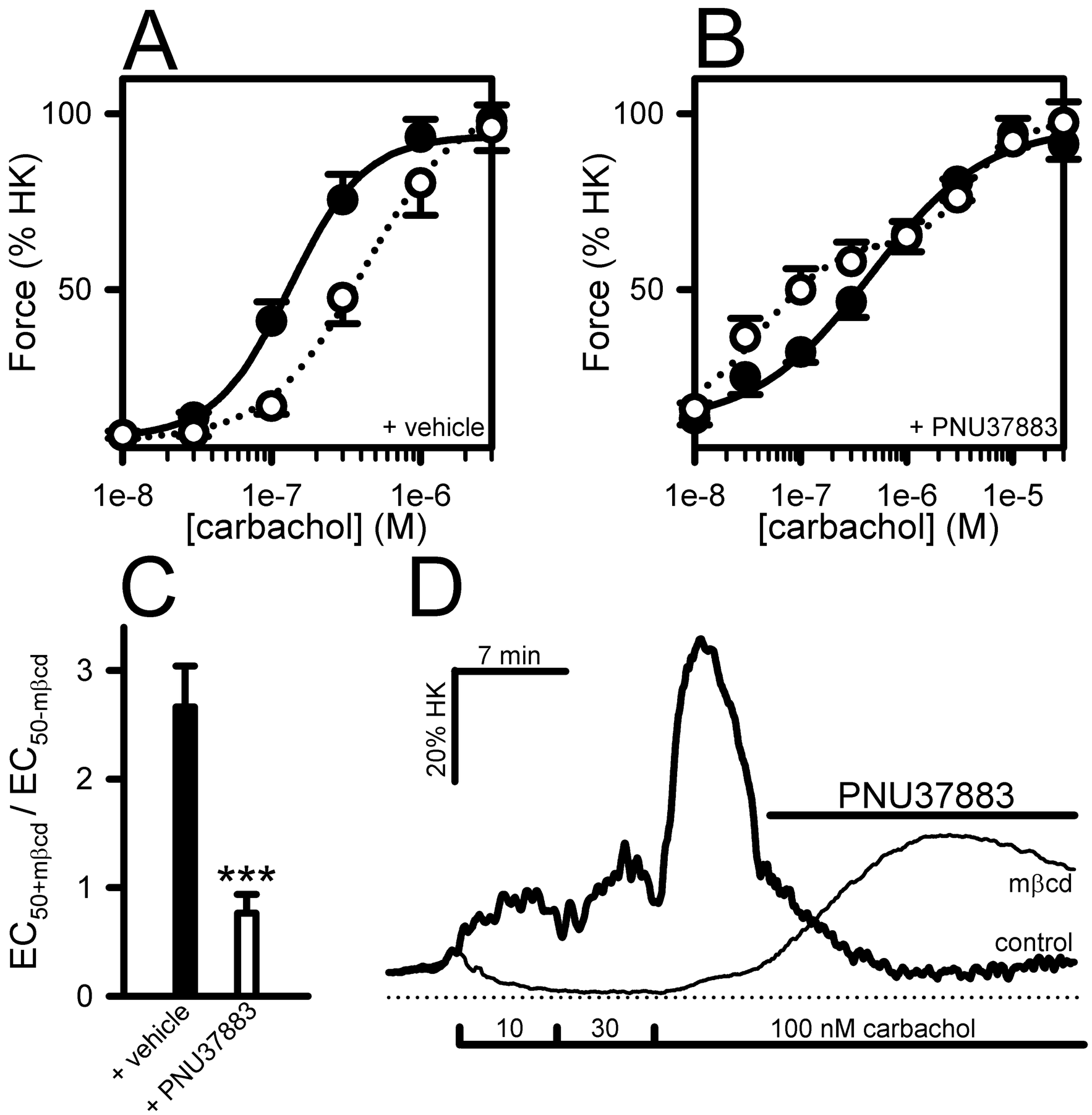
A
100
50
Force (% HK)
+ vehicle
1e-8
1e-7
1e-6
[carbachol] (M)
B
100
50
Force (% HK)
+ PNU37883
1e-8
1e-7
1e-6
1e-5
[carbachol] (M)
C
3
2
1
0
EC50+mβcd / EC50-mβcd
***
+ vehicle
+ PNU37883
D
7 min
20% HK
PNU37883
mβcd
control
10
30
100 nM carbachol

A

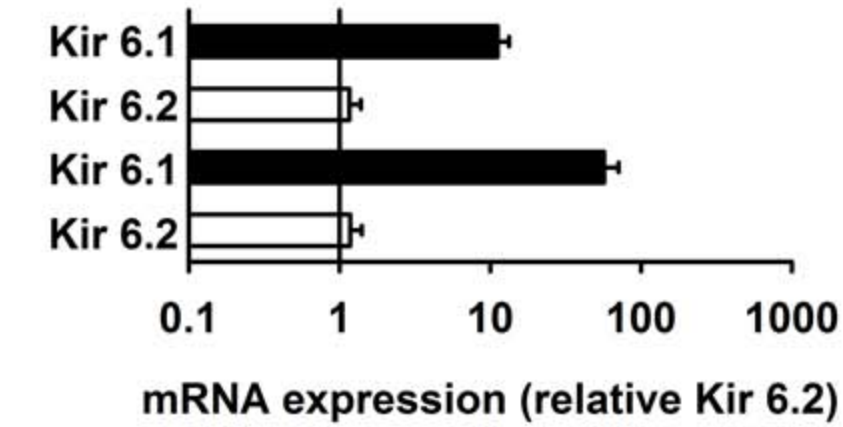
Kir 6.1
Kir 6.2
Kir 6.1
Kir 6.2
0.1
1
10
100
1000
mRNA expression (relative Kir 6.2)

B

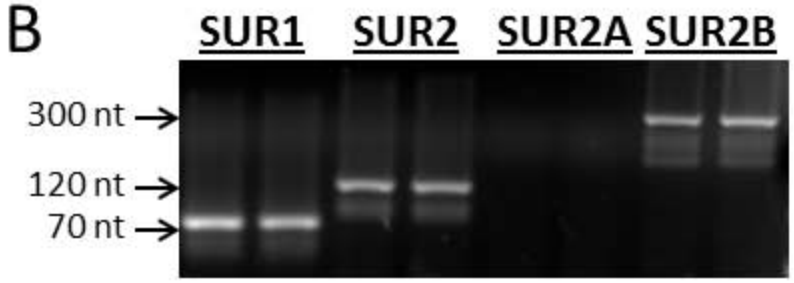
SUR1
SUR2
SUR2A
SUR2B
300 nt
120 nt
70 nt


A
Human bladder
Mouse aorta
kDa
37
Kir6.1
30
40
50 μg
30
40
50 μg
B
20
Cav-1
75
M3
50
Kir6.1
20
SM22α
1
2
3
4
5
6
7
8
9
10
12

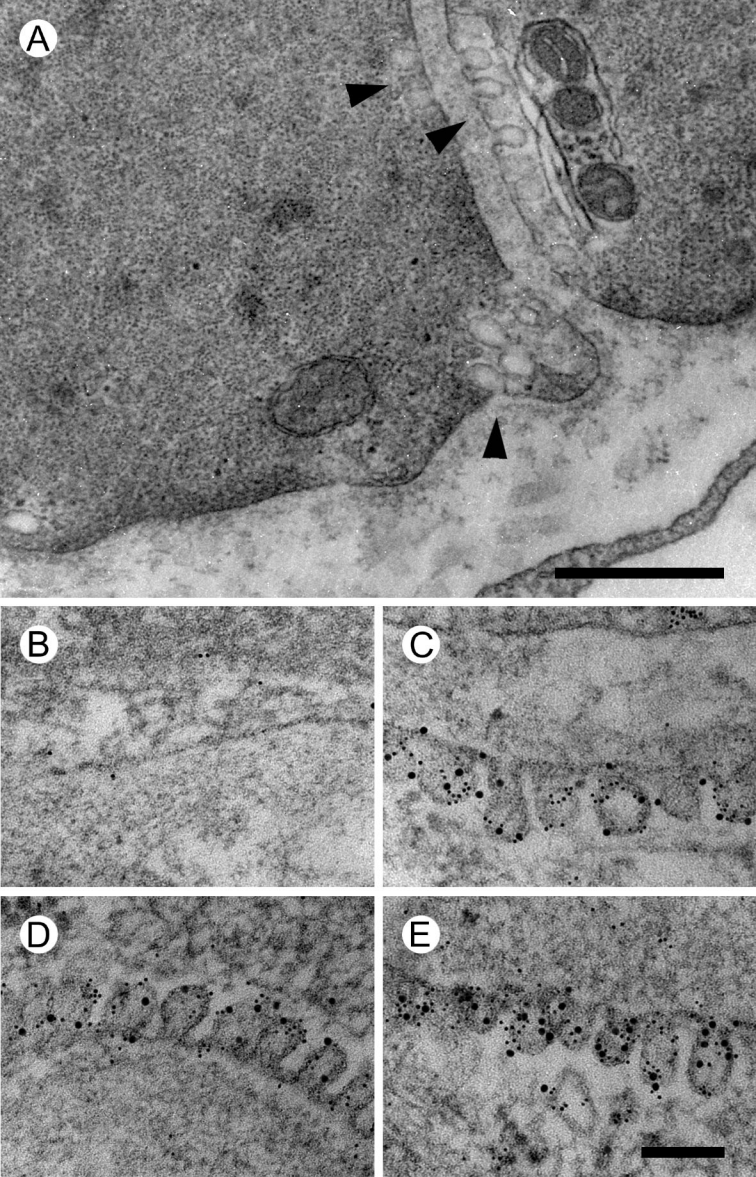
A
B
C
D
E

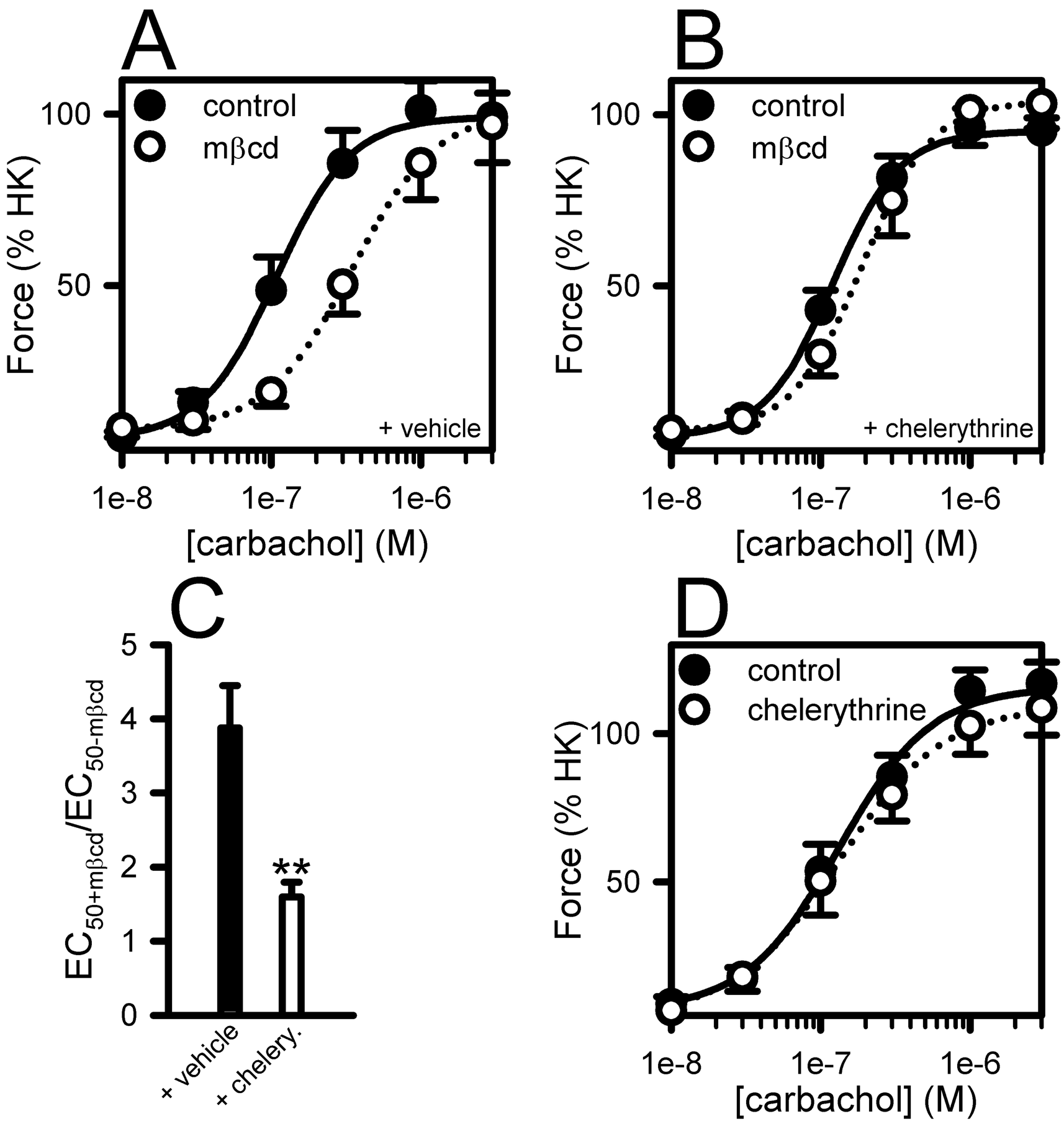
A
control
mβcd
100
50
Force (% HK)
+ vehicle
1e-8
1e-7
1e-6
[carbachol] (M)
B
control
mβcd
100
50
Force (% HK)
+ chelerythrine
1e-8
1e-7
1e-6
[carbachol] (M)
C
5
4
3
2
1
0
EC50+mβcd/EC50-mβcd
**
+ vehicle
+ chelery.
D
control
chelerythrine
100
50
Force (% HK)
1e-8
1e-7
1e-6
[carbachol] (M)